Oscillatory magnetotransport in the layer compounds $4Hb$-TaS_2 and $2H$-$TaSe_2$†*

R. M. Fleming and R. V. Coleman
Department of Physics, University of Virginia, Charlottesville, Virginia 22901
(Received 14 February 1977)

Quantum oscillations have been observed in the magnetoresistance and Hall effect of $4Hb$-TaS_2 and $2H$-$TaSe_2$ in fields up to 230 kG. For magnetic fields perpendicular to the layers at least twelve frequencies in the range 0.044 to 8.2 MG have been observed in $4Hb$-TaS_2. Eleven frequencies in the range 1.6 to 44.6 MG have been observed in $2H$-$TaSe_2$. The angular dependence of the frequencies generally follows functions of the form $\omega_\perp/\sin\theta$, where $\omega_\perp$ is the frequency observed for field perpendicular to the layers and θ is the angle between the field and the layers. The angular dependence is consistent with that expected for a nearly two-dimensional cylindrical Fermi surface and the small cross sections corresponding to the observed frequencies indicate that the Fermi-surface sections result from the $3a_0 \times 3a_0 \times c_0$ charge-density-wave superlattice. Maxima in the magnetoresistance rotation diagrams indicate the presence of open orbits along the c axis in both materials. Features in the field dependence of the magnetoresistance and Hall effect of $4Hb$-TaS_2 suggest the presence of magnetic breakdown while the field dependence observed in $2H$-$TaSe_2$ is well behaved although magnetic breakdown may play a role in the orbits associated with the highest frequencies.

I. INTRODUCTION

Layer-structure dichalcogenide crystals exhibit a large anisotropy in their electronic properties and the crystal structure suggests that the Fermi-surface topology should exhibit a two-dimensional character. This Fermi-surface geometry favors the formation of charge-density waves[1,2] (CDW's) in many of the phases and this is expected to modify the Fermi surface substantially at temperatures below the CDW transition. Energy gaps are introduced by the CDW and the new Fermi surface can be viewed as arising from the band folding required by the introduction of a new Brillouin zone characterizing the CDW superlattice. In order to obtain direct information on the Fermi-surface topology in these materials, we have attempted to measure high-field galvanomagnetic effects. These include quantum oscillatory components of the magnetoresistance and Hall resistivity as well as the overall field dependence of these quantities in magnetic fields up to 230 kG. We have grown crystals of approximately five different phases of the selenide and sulfide layer-structure crystals showing CDW transitions and have reported measurements[3] of the magnetoresistance and Hall effect in fields to 230 kG. Two of the materials, $4Hb$-TaS_2 and $2H$-$TaSe_2$ have been of sufficient perfection to show substantial quantum oscillatory behavior and preliminary results[4] have been reported for $4Hb$-TaS_2. The growth of these highly perfect crystals has been reproducible and has allowed us to make a complete set of measurements. This paper will review the experimental results and analyze them in terms of the Fermi-surface sections and the CDW effects that can be expected to play a role in the electronic properties of these two phases.

The general structure of these layer compounds[5] is a series of chalcogen-metal-chalcogen sandwiches separated by Van der Waals gaps. The sandwiches exhibit either trigonal prismatic or octahedral coordination of the metal atoms. $2H$-$TaSe_2$ contains two sandwiches per unit cell and has trigonal prismatic coordination. $4Hb$-TaS_2 has four sandwiches per unit cell with alternating octahedral and trigonal prismatic coordination. Details of the crystal structures and charge-density-wave transitions can be found in Refs. 1 and 5.

II. EXPERIMENTAL TECHNIQUES

dc magnetoresistance measurements were made on single crystals of $4Hb$-TaS_2 and $2H$-$TaSe_2$. The crystals were obtained by the method of iodine vapor transport from stoichiometric prereacted powders. $4Hb$-TaS_2 single crystals were grown in a gradient of 720–700 °C for 4–5 weeks. At the end of the growth period the crystals were quenched to room temperature. The crystals grew in the shape of three-dimensional polyhedra of hexagonal symmetry. The top and bottom basal-plane facets of the crystals had mirror surfaces while the sides had finely stepped surfaces reflecting the layered structure of the crystal. The largest crystals were about 3 mm in diameter by 2 mm thick. Measurements of the residual-resistance ratio [(RRR), $\rho_{300\,K}/\rho_{4.2\,K}$] were variable because of the large temperature dependent conductivity anisotropy. In the best specimens we estimate RRR to exceed 200.

Measurements on $2H$-$TaSe_2$ were made using

specimens provided by Bell Laboratories and crystals grown at the University of Virginia. The Bell crystals had dimensions on the order of $1\times2\times0.2$ mm with a RRR of 90–100. The Virginia crystals were grown in a gradient of 770–750 °C for 2 weeks. At the end of the growth period they were cooled to room temperature over a period of 12 h. The crystals grew in the shape of thin platelets with mirror surfaces. The largest crystals in the growth were about $1\text{ cm}\times1\text{ cm}\times0.05$ mm. Measurements on smaller, mounted specimens gave a RRR of 300. The magnetoresistance measurements on the two sets of specimens gave magnetoresistance values consistent with these ratios.

The crystals were mounted on prepared printed-circuit blocks using solder or silver-paint contacts. The most reliable leads were made using small silver paint contacts on the specimen with 50 AWG wire between the contacts and the circuit block to minimize strain. The majority of the measurements were made with the current parallel to the layers ($\vec{J}\perp\vec{c}$) although measurements were also made with the current perpendicular to the layers ($\vec{J}\parallel\vec{c}$). Measurements were made with the potential leads in both a standard resistance configuration and transverse to the current in a Hall configuration. Because of the three-dimensional geometry and the anisotropy in the conductivity of the as-grown $4Hb$-TaS_2 specimens, the current density was not generally uniform over the cross section of these crystals. Therefore, measurements on $4Hb$-TaS_2 were made with potential leads in the plane of the current leads and also with potential leads on the top facet of the crystal. The potential lead arrangements used on $4Hb$-TaS_2 are schematically illustrated in Fig. 1. Additional measurements were made on cleaved specimens of $4Hb$-TaS_2 where the geometry favored a more-uniform current density.

In general, a two-lead potential measurement of either the magnetoresistance or Hall voltage contains a mix of the two components due to imperfect alignment of the leads. Therefore, a standard four-term analysis is employed to separate the terms as well as to identify possible thermal or inductive contributions to the measured potential. In such an analysis four magnetic field sweeps are recorded corresponding to $\pm\vec{I}$ and $\pm\vec{B}$ and the measured voltages are decomposed into four terms as defined below:

$$V_R = A - B + C - D$$

(the magnetoresistive voltage),

$$V_H = A - B - C + D$$

(the Hall voltage),

$$V_I = A + B - C - D$$

(the inductive voltage),

$$V_T = A + B + C + D$$

(the thermal voltage), where

$$A = V(+\vec{I}, +\vec{B}),\quad C = V(+\vec{I}, -\vec{B}),$$
$$B = V(-\vec{I}, +\vec{B}),\quad D = V(-\vec{I}, -\vec{B}).$$

In order to determine the frequency of the oscillatory portion of the magnetoresistance, the semiclassical background resistivity (ρ_{sc}) was first estimated by making a third-order polynomial fit to the data. The quantity $\Delta\rho/\rho_{sc} = [\rho(B) - \rho_{sc}]/\rho_{sc}$ was calculated and plotted as a function of $1/B$. Frequency analysis was then performed using two methods. When only a few frequencies were present, a plot of the extremum number versus $1/B$ was made. In this case, the frequency is given by the slope of a linear fit to the data. For all cases including the complicated spectra a Fourier transform was also performed on an off-line computer. The analog data was converted to a set of digital points whose spacing was chosen to give a frequency resolution on the order of ±0.1 MG. In cases where a comparison between the graphical method and the Fourier transform could be made, excellent agreement between the two methods was obtained.

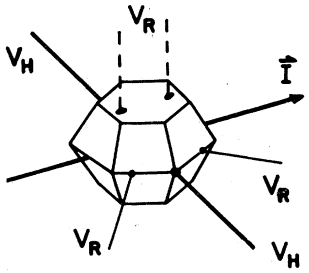

FIG. 1. Schematic representation of the lead arrangement used on the majority of the as-grown $4Hb$-TaS_2 crystals. V_R is the potential lead used for magnetoresistance measurements. V_H is the potential lead used for Hall measurements.

III. EXPERIMENTAL RESULTS

Because of the three-dimensional polyhedral shape of the $4Hb$-TaS_2 crystals and the anisotropies present in the conductivity of the layered compounds the direct experimental voltages measured in these experiments generally contain contributions from several components of the resistivity tensor. As described in the experimental section these contributions have been separated in a standard four-term analysis and oscillatory behavior is generally present in all components of the resistivity tensor. In addition, the $4Hb$-TaS_2 results show oscillatory components that do not behave as ordinary components of the resistivity tensor upon reversal of the field and current. This behavior

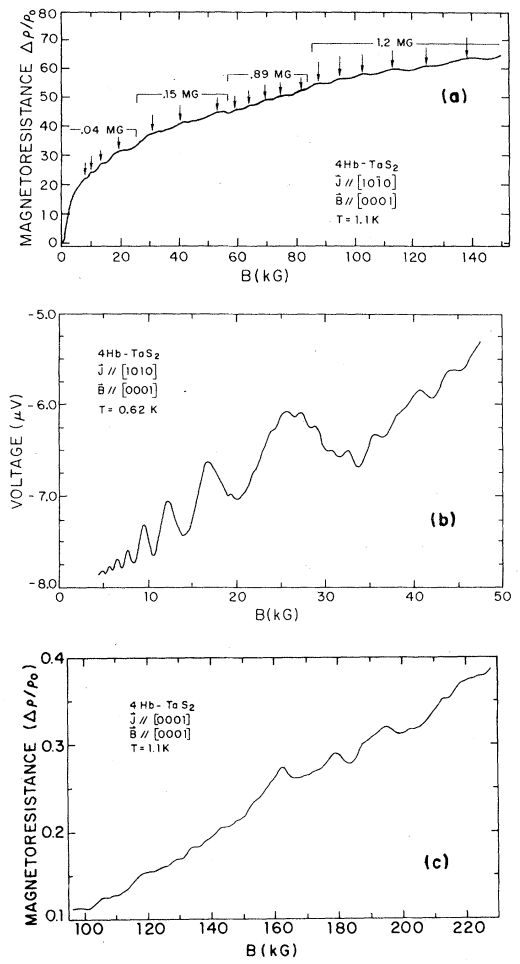

FIG. 2. Magnetoresistance curves measured for $4Hb$-TaS_2 with $\vec{B}$ parallel to the c axis. (a) $\vec{B}=0-150$ kG, $T=1.2$ K, arrows indicate positions of maxima. (b) $\vec{B}=0-50$ kG, $T=0.62$ K; (c) $\vec{B}=95-215$ kG, $T=1.2$ K.

appears to be connected with the extreme anisotropy of the $4Hb$ phase and will be outlined in further detail in Sec. III C. No effects of this type have been observed in the $2H$-$TaSe_2$ crystals. The frequencies observed for the oscillatory components show complete consistency and do not depend on which component shows the dominant oscillatory amplitude in a particular measurement. We will therefore first present the data on the oscillatory behavior and frequency analysis for $4Hb$-TaS_2 and $2H$-$TaSe_2$. In Sec. III C, we will examine the more-detailed behavior of the particular voltage components in $4Hb$-TaS_2.

A. Oscillatory transport in $4Hb$-TaS_2

Measurements have been made for a number of lead geometries. These include cases where the magnetoresistive voltage should dominate and cases where the Hall voltage should dominate. A typical magnetoresistance curve for $\vec{B}$ parallel to the c axis is shown in Fig. 2(a) for a field sweep from 0 to 150 kG at 1.2 K. Oscillatory components with frequencies in the range 0.04 to 1.2 MG have been observed. Within a particular range of magnetic field one major frequency appears to show the dominant amplitude in the direct field plots. However, Fourier transform analysis can generally detect a number of frequencies for all field ranges above 20 kG. The lowest frequency of 0.044 MG has been studied over a range of temperatures and is the only frequency observed below approximately 20 kG. The amplitudes of the oscillations are strongly temperature dependent and grow rapidly at lower temperatures as shown in Fig. 2(b) for a temperature of 0.62 K. Analysis of the lowest-frequency component has also been used to obtain an estimate of the effective mass and Dingle temperature and this will be discussed in Sec. IV.

In the field range 150–230 kG the quantum oscillations, although fairly large in amplitude, show an irregular behavior as shown in Fig. 2(c). A plot of the oscillatory magnetoresistance as a function of $1/B$ with the dc background magnetoresistance subtracted out is shown in Fig. 3(a). Only a few frequencies can be clearly identified in the direct field plot; however, the Fourier-transform analysis as shown in Fig. 3(b) gives a reproducible set of at least six frequencies in the range 1.2 to 8 MG. The full range of frequencies observed for $\vec{B}$ perpendicular to the layers is listed in Table I. In the overlap region of the high- and low-field data shown in Figs. 2(a) and 2(c) a frequency of ~1.2 MG is identified in each case giving a further check on the consistency of the frequency analysis in both field ranges. The amplitude variation of the oscillations at high fields can result from a complex beat structure or it could also be influenced by magnetic breakdown for particular orbits and this will be discussed further in Sec. IV A. For $\vec{B}$ perpendicular to the layers the magnetoresistance curves show substantially different slopes above and below 30 kG. This also suggests the presence of magnetic breakdown and further evidence will be presented below in reference to the Hall effect results on $4Hb$-TaS_2.

The angular dependence of the frequencies has been studied by recording field sweeps for field directions at successive angles between perpendicular and parallel to the layers. For the various field ranges a number of frequencies can be tracked in the direct-field plots. These can be determined graphically and followed as a function of angle. They are in agreement with the results of Fourier analysis which show the same frequencies

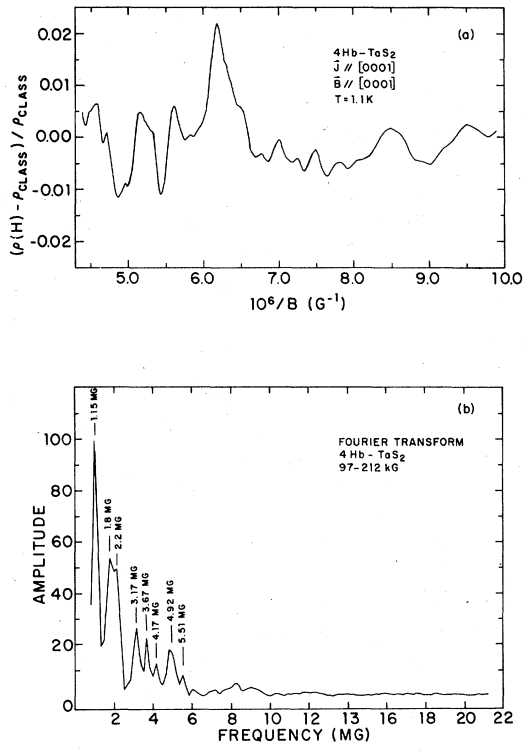

FIG. 3. (a) Oscillatory portion of the longitudinal magnetoresistance measured in $4Hb$-TaS_2 as a function of $1/B$. Magnetic field and current are parallel to the c axis. Transverse magnetoresistance measurements with field parallel to the c axis and current in the basal plane give the same result. (b) Fourier transform of the $4Hb$-TaS_2 magnetoresistance curve shown in (a).

as well as quite a few more that are difficult to pick out in the direct-field plots. For angles below about 10° no well-defined oscillations have been observed in magnetic fields from 0 to 230 kG.

As the field is rotated away from the perpendicular the frequencies increase and generally scale with angle according to the relation $\omega_\perp/\sin\theta$ as shown in Figs. 4(a) and 4(b). $\omega_\perp$ is the frequency observed for the perpendicular field direction and θ is the angle between the field and the layers. This is the angular dependence one would expect for cylindrical sections of Fermi surface with the axis of the cylinder parallel to the c axis.

The most complete angular data have been obtained for the lowest frequency and for this piece the cross section does not seem to deviate from $\omega_\perp/\sin\theta$ dependence by more than a few percent. However, the Fourier transform analysis does indicate a distinct frequency with a value (10–20)% lower than 0.044 MG. This may represent a second extremum on this cylinder although a precise value has not been determined since such a close pair of frequencies is at the limit of resolution of our present Fourier-transform program.

The higher frequencies also scale up as the field is rotated away from the perpendicular direction and many of them follow fairly closely to the function $\omega_\perp/\sin\theta$. It is possible that a number of these should be paired together and associated with a maximum and a minimum on the same undulating cylinder. Extensive additional data particularly at lower angles will be required in order to decide on a precise pairing.

In the low-frequency range 0.044–0.24 MG a number of data points have been obtained in the Fourier transform analysis which indicate the presence of harmonics of the 0.044-MG frequency at 0.09, 0.13, and 0.17 MG for field perpendicular to the layers. These exist over a reasonable angular range, but limited data points and low amplitudes do not allow a complete analysis at present.

Sharp maxima have been observed in the magnetoresistance for currents parallel and perpendicular to the layers. The most convincing evidence connecting these maxima with open orbits has been obtained for current perpendicular to the layers and field in the basal plane as shown in Fig. 5. The field dependence at the maximum follows a relation $\Delta\rho/\rho_0 \sim B^n$ with $n \sim 1$ while for other field directions $n < 1$ and the magnetoresistance tends to saturation at high fields. Assuming an uncompensated metal these results indicate open orbits along the c axis. Band-structure calculations[1] for the $1T$ and $2H$

TABLE I. Frequencies identified in $4Hb$-TaS_2 for $\vec{B} \parallel [0001]$.

Shubnikov–de Haas area (10^{-2} Å^{-2})	Shubnikov–de Haas frequency $\omega_\perp$(MG)	
0.042	0.044	FT, [a] G [b]
0.16	0.17	FT, G
0.23	0.24	FT
0.34	0.36	FT
0.46	0.48	FT, G
0.85	0.89	FT, G
1.12	1.18	FT, G
1.72	1.8	FT
2.1	2.2	FT
3.0	3.2	FT
3.4	3.6	FT
4.0	(4.2) [c]	(FT)
4.7	4.9	FT
5.2	(5.5) [c]	(FT)
7.8	8.2	FT

[a] FT is the Fourier-transform analysis used to determine frequency.

[b] G is the graphical construction used to determine frequency.

[c] (FT) are the frequencies that appear in Fourier transform with only weak amplitude.

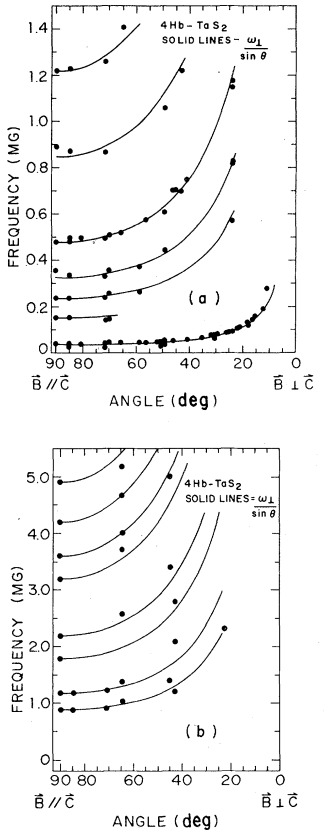

FIG. 4. Angular dependence observed for 13 frequencies in $4Hb$-TaS_2. The angles are measured between the magnetic-field direction and the basal plane. The solid lines represent functions of the form $\omega_\perp/\sin\theta$ where $\omega_\perp$ is the frequency observed at $\theta=90°$. This function would be followed exactly for a section of Fermi surface which is a perfect cylinder with the axis parallel to c. (a) Data for the seven lower frequencies in the range 0.044–1.2 MG. (b) Data for the higher frequencies in the range 0.8–4.9 MG.

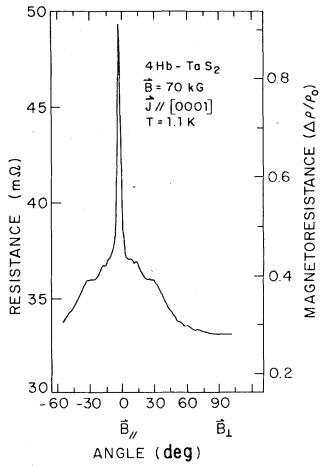

FIG. 5. Magnetoresistance rotation diagram for $4Hb$-TaS_2 obtained in a magnetic field of 70 kG. Current is parallel to the c axis and field is rotated from the longitudinal to the transverse orientation in the $(11\bar{2}0)$ plane. The sharp maximum is observed for field in the basal plane and current along c indicating the presence of open orbits along the c direction.

phases show the conduction arising from a half-filled d band and would indicate an uncompensated behavior unless unusual changes occur in the CDW state and the $4Hb$ phase. As the field is rotated from the transverse to longitudinal orientation oscillations identified with the three lowest frequencies are observed and the analysis of the period spacing with angle shows them to be consistent with a $\omega_\perp/\sin\theta$ dependence of the cross section.

Transverse-magnetoresistance rotation diagrams have also been recorded with the current in the basal plane and an example taken in a field of 211 kG is shown in Fig. 6. For field directions parallel to the basal-plane maxima are observed at high fields. Below 100 kG these same field directions correspond to minima in the rotation diagrams consistent with the magneotresistance behavior observed previously for other layer structure crystals.[3] The maxima shown in Fig. 6 develop for fields above 100 kG and the field dependence in this field range is approximately linear in contrast to other field directions where a trend toward saturation is observed. While these maxima are consistent with open orbits parallel to the basal plane the transition from minima to maxima and the extreme crystal anisotropy suggest that further checks will be necessary. In addition, the observed field dependence is not completely resolved in terms of the expected high-field limit

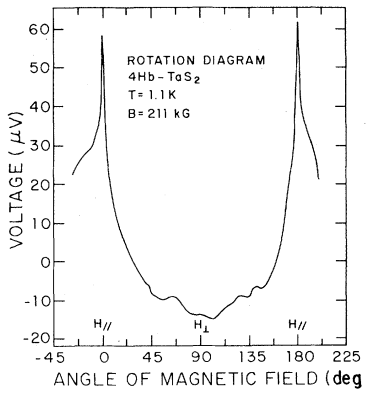

FIG. 6. Transverse-magnetoresistance rotation diagram with current parallel to the basal plane. The field is rotated in the $(1\bar{2}10)$ plane and the maxima occur for field parallel to the layers and perpendicular to the current. For field perpendicular to the layers the voltage is negative due to a Hall contribution.

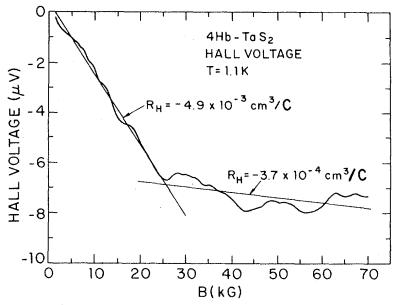

FIG. 7. Field dependence of the Hall voltage in $4Hb$-TaS_2 at 1.1 K. The straight lines have been used to estimate the dc Hall coefficient in the two field ranges. The abrupt change in slope at ~ 25 kG is attributed to magnetic breakdown.

behavior.

Below about 25 kG the Hall voltage is reasonably linear with the 0.044 MG frequency superimposed. At 25 kG there is a sharp break in slope and several new frequencies appear. The break in slope indicates an abrupt change in the Hall coefficient as calculated from the slope, $R_H \propto \Delta V/\Delta B$. The magnitude of the Hall coefficient has been calculated by using straight-line fits to sections of the Hall voltage between 0 and 70 kG as shown in Fig. 7. For fields from 0 to 30 kG, $R_H = -4.9\times10^{-3}$ cm^3/C, while from 30 to 70 kG, $R_H = -3.7\times10^{-4}$ cm^3/C. The initial value of the Hall coefficient is anomalously large and the order-of-magnitude decrease above 25 kG gives a value of the Hall coeffiecient above 25 kG more characteristic of previous measurements on other layer compounds.[3,6] At much higher fields the Hall voltage continues to show a nonlinear field dependence and above 80 kG the slope becomes slightly positive although exact values are difficult to estimate due to the large oscillatory components. The negative Hall voltage measured at helium temperatures in the above experiments develops at temperatures below the onset of the CDW at 28 K in the trigonal prismatic layers.

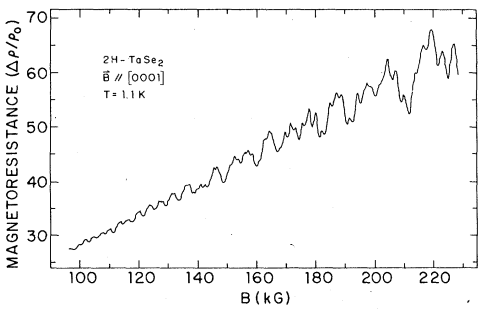

FIG. 8. Transverse magnetoresistance observed for $2H$-$TaSe_2$ in the field range 95–230 kG. The magnetic field is perpendicular to the layers and the current is parallel to the layers. The dc background magnetoresistance is monotonic with no major indication of magnetic breakdown up to 230 kG.

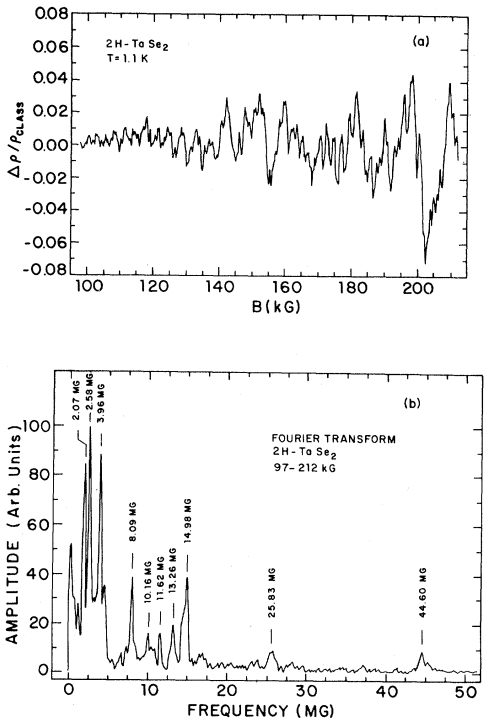

FIG. 9. (a) Oscillatory component of the Hall lead voltage observed in $2H$-$TaSe_2$ from 95 to 230 kG. Magnetic field is parallel to the c axis. The closely spaced oscillations above 200 kG arise from the 44.6-MG frequency. (b) Fourier transform of the $2H$-$TaSe_2$ Hall lead data shown in (a).

B. Oscillatory transport in $2H$-$TaSe_2$

Magnetoresistance and Hall resistivity have been measured in single crystals of $2H$-$TaSe_2$ with RRR in the range 90–300. Quantum oscillations are observed in fields above ~ 50 kG for the highest ratio crystals and all crystals have shown substantial oscillations above 100 kG. A magnetoresistance sweep in the field range 95–230 kG for field perpendicular to the layers and current parallel to the layers is shown in Fig. 8. A large number of frequencies are present in the data of Fig. 8 and similar behavior is observed for leads in the Hall configuration as shown in Fig. 9(a). The monotonic background increase of voltage with field has been subtracted out from the curve of Fig. 9(a) using a third-order polynomial fit to the background. A number of individual frequencies can be identified and tracked in this curve and the frequencies have been determined from a direct plot of period number versus $1/B$ and also from a Fourier transform analysis of paper tape data as

TABLE II. Frequencies identified in $2H$-$TaSe_2$ for $\vec{B} \| [0001]$.

Orbit	Calculated[a] frequency $\omega_\perp$(MG)	de Haas–van Alphen[b] frequency $\omega_\perp$(MG)	Shubnikov–de Haas frequency $\omega_\perp$(MG)	Shubnikov–de Haas area (10^{-2} Å^{-2})
	0.81			
	0.91			
α	1.8[c]	1.62	1.6	1.5
γ		2.30	2.1	2.0
β		2.57	2.6	2.5
δ	3.63	3.98	4.0	3.8
	7.2			
ϵ	8.9	8.00	8.1	7.7
η		10.1	10.2	9.7
κ			11.6	11.0
λ			13.3	12.7
	13.8[c]			
μ		14.9	15.0	14.3
ζ	23.9[c]	24.5	25.8	24.6
σ	36.9[c]		44.6	42.6

[a] From model of Scott and Rice (Ref. 17) calculated for purely two-dimensional band.
[b] Graebner (Ref. 7).
[c] Orbits resulting from possible magnetic breakdown in model of Scott and Rice.

shown in Fig. 9(b). Reasonably good agreement is obtained between the two methods and the individual identified frequencies for field perpendicular to the layers are shown in Table II. The Hall voltage for $2H$-$TaSe_2$ is nonlinear in magnetic field but a reasonably smooth rising background is observed with no abrupt changes in slope. At lower fields in the range 0–100 kG smooth curves are also observed with evidence of oscillatory behavior first developing above ~50 kG. In general, the data do not show the strong evidence of magnetic breakdown that was observed in $4Hb$-TaS_2 and this point will be discussed further in Sec. IV.

A limited number of runs have been recorded for fields at angles between perpendicular to the layers and 45° off perpendicular. Fourier analysis of these runs has given frequencies that agree with the more complete angular dependence obtained from the de Haas–van Alphen measurements by Graebner.[7] The magnetoresistance frequencies are plotted in Fig. 10 along with the de Haas–van Alphen results obtained by Graebner.[7] The solid lines are plotted according to the function $\omega_\perp/\sin\theta$. The lower frequencies deviate in pairs from these curves for field directions near perpendicular while they merge into a single frequency at angles 50–60° off the perpendicular direction. Graebner assigns these pairs to extrema on the same undulating cylinder.

Crystals with current oriented perpendicular to the layers ($\vec{J} \| \vec{c}$) have also been measured in a magnetoresistance configuration. A transverse to longitudinal rotation diagram shows sharp peaks for magnetic field directions parallel to the layers as would be expected for open orbits parallel to the c axis in an uncompensated metal. The field dependence shows an exponent n in the relation $\Delta\rho/\rho \sim B^n$ of ~1 with a slightly lower coefficient observed at adjacent field directions. This is

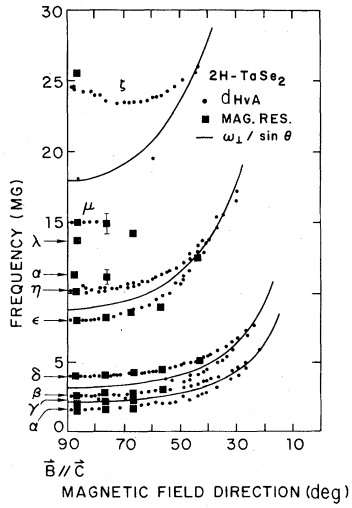

FIG. 10. Angular dependence of the frequencies observed in $2H$-$TaSe_2$ from both Shubnikov–de Haas and de Haas–van Alphen experiments. The de Haas–van Alphen results were obtained by Graebner (Ref. 7). The solid lines are functions of the form $\omega_\perp/\sin\theta$, where $\omega_\perp$ is the frequency at $\theta = 90°$ corresponding to the average of the two paired branches.

consistent with the existence of open orbits along $\vec{c}$, but even at 230 kG the high-field-limit behavior is not fully observed. Hambourger[8] has claimed evidence for open orbits in the c axis direction in $2H$-$TaSe_2$; however he has assumed the $2H$ phase to be compensated in his analysis. The addition of a second sandwich per unit cell in the $2H$ phase causes appreciable d-band splitting away from the basal planes and modifies the Fermi surface from that of the $1T$ phase, however no major change in compensation state would be expected in the present model.

The four-term analysis of the above data has shown the oscillatory terms to be in the standard magnetoresistivity and Hall-resistivity terms of the resistivity tensor. Reversal of current and field directions has produced no unusual behavior for any of the lead configurations in contrast to the measurements on $4Hb$-$TaSe_2$ as discussed below.

C. Anomalous oscillatory voltages

Magnetoresistance measurements on thick as-grown specimens display an anomalous oscillatory voltage component which does not reverse with current direction. This behavior appears to be connected with the extreme conductivity anisotropy in $4Hb$-TaS_2 which results in tunneling conductivity along the c axis[9] and introduces a large current inhomogeneity. The frequencies and general analysis in terms of Fermi-surface topology do not appear to be affected by these unusual phase effects, but they are sufficiently prominent that a careful summary is in order.

For the thick as-grown crystals a four-term analysis of the potentials measured for various pairs of leads give anomalous oscillatory components which do not depend on the direction of the current. They depend linearly on the magnitude of the current and the amplitude grows with magnetic field as expected for a standard Shubnikov–de Haas oscillation. Depending on lead geometry, these anomalous oscillatory components can show either an odd or an even dependence on field direction. The two cases are demonstrated in Fig. 11 where the lead configurations are indicated in the inserts. The curves shown in Fig. 11 show the conventional terms obtained from a combination of voltages measured for $\pm\vec{I}$ and $\pm\vec{B}$. The major amplitudes of oscillation occur in the terms that are even in $\vec{I}$ as opposed to the usual magnetoresistance and Hall terms which are odd in $\vec{I}$. Phenomenologically this can be described by allowing the phase of the oscillation to depend on the sign of the field and current. The magnetoresistance and Hall terms become relatively smooth in this type of analysis although evidence of oscillatory components is still seen.

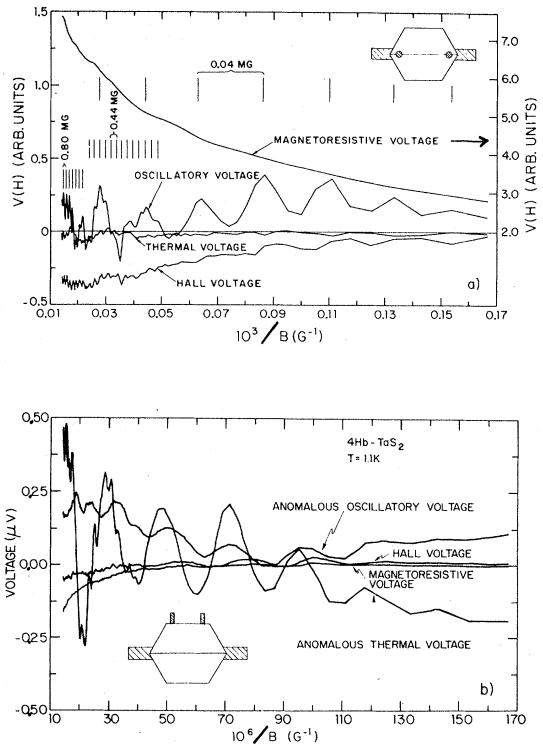

FIG. 11. Separated components of the voltage in $4Hb$-TaS_2 obtained by appropriate summing of the four terms $A = V(+\vec{I}, +\vec{B})$, $B = V(-\vec{I}, +\vec{B})$, $C = V(+\vec{I}, -\vec{B})$, and $D = V(-\vec{I}, -\vec{B})$ plotted against $1/B$. Lead configurations are shown in the inserts (also see Fig. 1). (a) Dominant oscillations occur in the term $A + B - C - D$ which is odd in $\vec{B}$ and dependent only on $|\vec{I}|$. (b) Dominant oscillations occur in the term $A + B + C + D$ which is even in $\vec{I}$ and $\vec{B}$.

Figure 11(a) shows data obtained with leads on the finely stepped side surfaces of the crystal in the same plane as the current leads. In this case the dominant oscillations are even in $\vec{I}$ and odd in $\vec{B}$. Figure 11(b) shows data obtained with leads on the top surface of the crystal. In this case the dominant oscillation is even in $\vec{I}$ and even in $\vec{B}$ as well. In the second case the Hall voltage and the magnetoresistive voltage are both very small as opposed to the case in Fig. 11(a) where they show a rapid increase in magnitude with field. This would indicate that in the second case the current may be significantly reduced in the layers adjacent to the surface on which the potential leads are placed.

If the three-dimensional crystals are cleaved into thin specimens so that a uniform cross section and a more-standard lead configuration and current distribution can be achieved, the oscillations revert to an odd dependence on current and appear in the standard magnetoresistance and Hall terms.

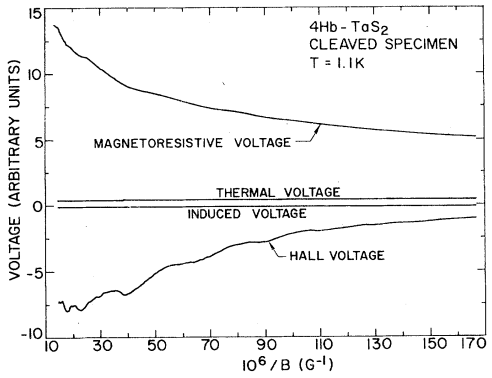

FIG. 12. Four-term analysis of the same type used for the data of Fig. 10 but applied to a thin-cleaved crystal of $4Hb$-TaS_2 where the geometry favors a more uniform current flow. In this case the dominant oscillations occur only in the magnetoresistance and Hall terms which are odd in $\vec{I}$.

The results of a four-term analysis for such a crystal are shown in Fig. 12. The terms even in $\vec{I}$ which are labeled thermal and induced are very small and essentially independent of magnetic field while the usual terms odd in $\vec{I}$ show oscillatory components and increase with field as expected.

IV. DISCUSSION

The frequencies of the oscillatory terms have been determined by plotting extremum number versus inverse field and calculating a linear fit to the data and by Fourier-transform analysis. The linear fits have been quite satisfactory for the low frequencies while the Fourier transforms have been required for the more-complex high-field data. If the quantum oscillations result only from oscillations in the density of states and do not contain contributions from magnetic breakdown and electron interference effects then the usual theoretical treatments apply and expressions describing the transverse magnetoresistivity $\rho(B)$ can be obtained as follows[10]:

$$\rho(B) = \rho_{sc}\left\{1 + \frac{5}{2}\sum_{r=1}^{\infty} b_r \cos\left[2\pi\left(\frac{F}{B}\right) - \frac{\pi}{4}\right] + R\right\}. \quad (1)$$

ρ_{sc} is the nonoscillatory portion of the magnetoresistivity, b_r is a term which includes the temperature and collision broadening of the levels, F is the frequency of oscillation, B is the magnetic field, and R is a term that represents the contribution of intralevel scattering. The relative importance of R depends on the ratio of the width of the Landau level Γ to the Fermi energy E_F, and is usually unimportant when the collisions are frequent enough to damp out the higher harmonics.

The most immediate information which can be obtained from a magnetoresistance experiment in the quantum regime is a measure of the extremal cross section of the Fermi surface, and this information is extracted from a measurement of the frequency of the oscillations. In special cases where the background magnetoresistance ρ_{sc} is well characterized and where magnetic breakdown effects are unimportant information on effective mass and Dingle temperature can be extracted. The Dingle temperature results from a broadening of the Landau levels due to collisions and is given by

$$T_D = \Gamma/\pi k_b = h/2\pi k_b \tau, \quad (2)$$

where Γ is the halfwidth of the Lorentzian line shape and τ is the relaxation time for collision.

The data obtained in the present experiments is sufficiently complex that the standard Shubnikov–de Haas theory can be applied only to a limited extent. Some information on effective mass and Dingle temperature has been extracted while a reasonably complete separation of the frequencies has been accomplished. The magnitude and number of resolved frequencies suggest a strong connection to the charge-density-wave state of the Fermi surface and these arguments along with a comparison to possible Fermi-surface models will be given in Sec. IV A. Calculations of effective mass and Dingle temperature as well as possible magnetic breakdown effects will be discussed in Sec. IV B and IV C.

A. Frequency analysis

The lowest frequencies observed in both $4Hb$-TaS_2 and $2H$-$TaSe_2$ would be estimated to arise from areas that represent less than 1% of the area of the Brillouin zone for the non-CDW state of the lattice. For $4Hb$-TaS_2 the lowest frequency of 0.044 MG corresponds to $\sim 3\times10^{-4}$ electrons per atom while for $2H$-$TaSe_2$ the lowest frequency of 0.8 MG corresponds to 6×10^{-3} electrons per atom. Band-structure calculations applying to the non-CDW lattice for $4Hb$-TaS_2 by Wexler and Woolley,[11] and for $2H$-$TaSe_2$ by Matheiss[12] and by Wexler and Woolley[13] indicate the existence of only large sections of Fermi surface containing approximately 10^{-1} electrons per atom with estimated frequencies above 20 MG. Sketches of the non-CDW Fermi surfaces[1] constructed from the band-structure calculations are shown in Fig. 13. The low values and the large number of frequencies observed for both materials measured in the present experiment suggest that the analysis should take into account the superlattice formed by the CDW.

In $4Hb$-TaS_2 two independent CDW transitions[1,14]

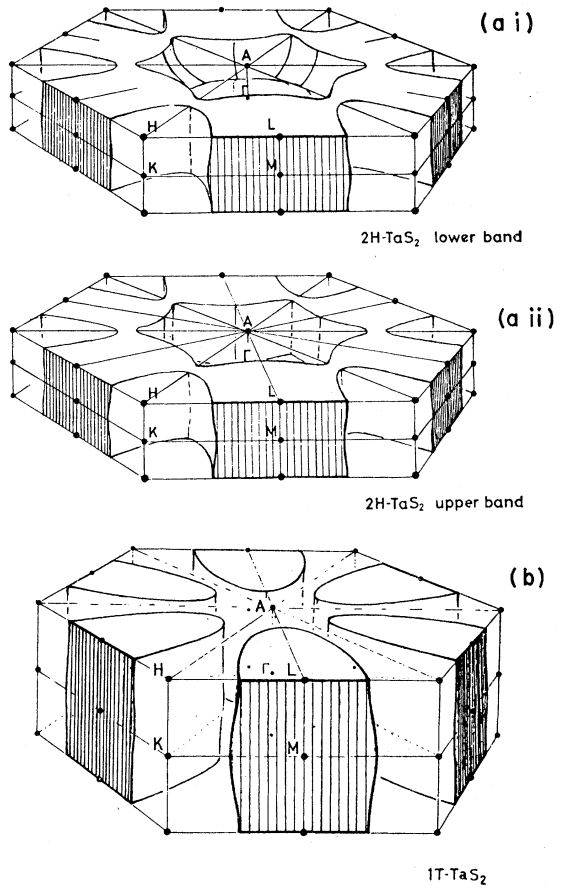

FIG. 13. Fermi-surface models constructed from the band-structure calculations for $2H$-TaS_2 and $1T$-TaS_2 in the non-CDW state (Ref. 1). The band structure of the $4Hb$-TaS_2 phase should be a superposition of these two models with a small amount of electron transfer. For both structures the non-CDW Fermi surfaces give only a few cross-sections corresponding to frequencies above 20 MG.

occur, one in the octahedral layers at 315 K and one in the trigonal prismatic layers at 21 K. In $2H$-$TaSe_2$ an incommensurate CDW forms at 120 K and becomes commensurate at 90 K.[15] In an analysis of Raman data on $2H$-$TaSe_2$ Holy *et al.*[16] have presented strong evidence for a $3a_0 \times 3a_0 \times c_0$ superlattice cell due to the superposition of three CDW's below the "lock-in" transition. In the case of $4Hb$-TaS_2 at helium temperatures the trigonal prismatic layers show a conductivity[9] three orders of magnitude greater than the octahedral layers indicating that the electron transport should be dominated by the effects of the CDW in the trigonal prismatic layers. The trigonal prismatic layers in the $4Hb$-TaS_2 should also support triple CDW's in the plane of the layers with $\lambda_{CDW} = 3a_0$. The superlattice Brillouin zone in $2H$-$TaSe_2$ and in the trigonal prismatic layers of $4Hb$-TaS_2 will therefore be reduced in area to $\frac{1}{9}$ of the original area in the plane parallel to the layers. The new Fermi surface would then be calculated by folding the band structure into the new zone in the presence of the triple CDW.

Scott and Rice[17] have carried out a preliminary band folding for a two-dimensional model of a triple-CDW state based on their saddle point mechanism[18] of CDW formation. They obtain sections of Fermi surface giving rise to frequencies estimated to be in the range 0.8–8 MG. Calculated frequencies from the model of Scott and Rice are listed in Table II. These are in qualitative agreement with the range of frequencies observed in the present experiments as listed in Tables I and II, although in both materials we identify more frequencies than predicted by the simple model of Scott and Rice. In $4Hb$-TaS_2 at least 12 frequencies in the range 0.8–8 MG are observed. The additional frequencies can come from pairs of frequencies on the same undulating cylinder or from breakdown orbits or higher harmonics as well as additional sections not present in the model. In the range 150–230 kG no new frequencies with values outside the range 0.04–8 MG appear to develop in $4Hb$-TaS_2. This might be interpreted to indicate that most of the existing sections of Fermi surface have already been seen at lower fields.

In $2H$-$TaSe_2$, the Shubnikov–de Haas and de Haas–van Alphen (dHvA) results agree on seven frequencies below 10 mG. Three pairs of these are identified with the same undulating cylinders so that rough agreement with the simple model is obtained. However, the Shubnikov–de Haas (SdH) results show additional frequencies at 11.6 and 13.3 MG and both experiments show higher frequencies (15, 25.8, and 44.6 MG—SdH) and (24,5 MG—dHvA). The high frequency of 44.6 MG might result from magnetic breakdown at symmetry points around the outside perimeter of the zone resulting in an orbit encompassing nearly the entire area of the reduced zone. In the de Haas–van Alphen results Graebner assigns the 14.9- and 24.5-MG frequencies to the same large undulating cylinder providing he assumes this section of Fermi surface is open along the c direction. In order to fit the model of Scott and Rice the ~25-MG frequency could come from magnetic breakdown involving several of the smaller sections. The interpretation of the ~15-MG frequency in this model is uncertain. It could involve magnetic breakdown or it could connect to the lower frequency of 13.3 MG identified as λ in the Shubnikov–de Haas results. The angular dependence of the Shubnikov–de Haas results is consistent with the pairing assigned by

Graebner (see Fig. 10).

In the case of $4Hb$-TaS_2, the extremely low frequency of 0.044 MG is unusually low even for a highly gapped Fermi surface. A low frequency such as this could result from a difference frequency between two larger sections of Fermi surface. Schlottmann and Falicov[19] have in fact considered de Haas–van Alphen oscillations in CDW systems and have shown that nonlinear effects can exist which would be expected to enhance the amplitude of the difference oscillations. Further experimental work will be required to check this possibility.

A more detailed band-structure calculation for the $4Hb$ phase will also be needed for comparison to the present experimental results. We have neglected the contribution of the octahedrally coordinated layers to the conductivity of $4Hb$-TaS_2. In general, the $4Hb$ band structure will be a superposition of the $2H$ and $1T$ band structures with a small amount of electron transfer from octahedral to trigonal layers estimated to be ~2% by Wexler and Woolley[11] and with some modification due to level repulsion. The CDW state in the $1T$ layers has a superlattice with $\lambda_{CDW} = 13a_0$ and a band folding into the corresponding reduced zone will also have to be accomplished. It is possible that Fermi-surface sections resulting from this folding will also contribute to the quantum oscillatory behavior although no definite evidence is available.

The well-behaved amplitude growth of the quantum oscillations in $2H$-$TaSe_2$ and the smooth monotonic increase with field of the background magnetoresistance and Hall resistance indicate that no major changes in orbit topology are occurring due to magnetic breakdown. Calculations by McMillan[20] show that a large CDW gap should be expected in $2H$-$TaSe_2$. This conclusion arises from a short coherence-length model which fits the specific-heat and neutron-diffraction results much better than the conventional long coherence-length theory which would predict considerably smaller gaps. For example the conventional theory predicts an energy gap $2\Delta(0) = 0.037$ eV while infrared measurements[21] indicate a CDW gap of 0.25 eV in $2H$-$TaSe_2$. From the estimates of the energy gap one can calculate the critical breakdown fields using expressions discussed below in Sec. IV C. The resulting values of critical breakdown field for the two gaps are given by $\vec{B}/\mu = 304$ kG and $\vec{B}/\mu = 1.4\times10^4$ kG, where $\mu = m^*/m_e$ is the effective-mass ratio. We have used a Fermi energy estimate of ~0.4 eV which has been estimated from the band-structure calculation[12] by measuring from the bottom of the conduction band to the Fermi level. If the latter estimate is correct we would not observe breakdown even for the light masses at 200 kG while the lower gap should break down well within our experimental field range.

B. Dingle temperature and effective mass

Experimentally, one may extract the effective-mass ratio from the temperature dependence of the amplitude of the oscillations and the Dingle temperature from the field dependence. The temperature dependence of the amplitude is given by

$$\frac{1}{T}\left(\frac{\Delta\rho}{\rho_{sc}}\right) \propto \frac{1}{\sinh(\lambda\mu T/B)} = 2e^{-\lambda\mu T/B} \times(1+e^{-2\lambda\mu T/B}+\cdots), \tag{3}$$

where $\lambda = 2\pi^2 m_0 c k_B/\hbar e = 146.9$ kG. For sufficiently large argument of the hyperbolic sine a plot of $\ln(\Delta\rho/T\rho_{sc})$ vs T will have a slope of $-\lambda\mu/B$. To calculate the Dingle temperature, one measures $\Delta\rho/\rho_{sc}$ as a function of field and plots $\ln[\Delta\rho/\rho_{sc})B^{1/2} \times\sinh(\lambda\mu T/B)]$ vs $1/B$. The slope is then $-\lambda\mu T_D$. Further details of this type of analysis are summarized by Anderson and Stone.[22] Using a value of $\mu \approx 0.07$ estimated from the temperature dependence data gives $T_D \approx 1$ K for the 0.044-MG frequency of $4Hb$-TaS_2. These numbers are subject to considerable uncertainty due to the fitting procedure. However, a check on the internal consistency can be made by using them to generate the field dependence of the low-frequency oscillation and then comparing the result to the observed magnetoresistance curve. Such a comparison is shown in Fig. 14 and the fit remains quite good over many cycles when the parameters $T_D = 1.4$ K and $\mu = 0.065$ are used.

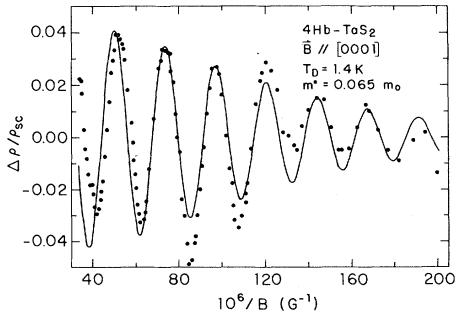

FIG. 14. Calculated oscillatory component of the magnetoresistance in $4Hb$-TaS_2 using the Dingle temperature of 1.4 K and the effective mass ratio $\mu = 0.065$ determined for the lowest frequency of 0.044 MG. Solid curve is the calculated curve and the dotted curve is the experimental curve. These parameters give a good fit over many cycles and confirm the estimates of T_D and μ for this orbit.

C. Magnetic breakdown

As pointed out in reference to $4Hb$-TaS_2 both the magnetoresistance and Hall effect show fairly abrupt changes in slope characteristic of the changes expected when magnetic breakdown is present and orbit topology is changed. They occur between 20 and 30 kG in the region where the low-frequency oscillation is approaching the quantum limit and only one Landau level should remain above 30 kG. This remaining level should give only one very broad period above 30 kG. Using the parameters μ and T_D calculated in the previous section a theoretical curve for the contribution to the magnetoresistance of the 0.044-MG frequency over the entire field range is shown by the solid curve in Fig. 15. The total measured magnetoresistance curve fits well to this curve below ~30 kG, but falls substantially below this curve at higher fields as might be expected if breakdown to larger more extended orbits has occurred and the exponent in the background magnetoresistance changes.

Magnetic breakdown can occur whenever $\hbar\omega_c \gg E_g^2/E_F$, where E_F is the Fermi energy. The probability of transition between orbits is given by[23]

$$P = \exp(-H_0/H), \tag{4}$$

where

$$H_0 \approx (E_g^2/E_f)(mc/e\hbar). \tag{5}$$

A semiclassical treatment of magnetic breakdown in the high-field limit has been given by Falicov and Sievert[24] who show that major modifications of the high-field behavior can be realized when an orbit undergoes magnetic breakdown from open to closed or vice versa, or if magnetic breakdown changes the compensation of the metal as in the case of magnesium and zinc.[25]

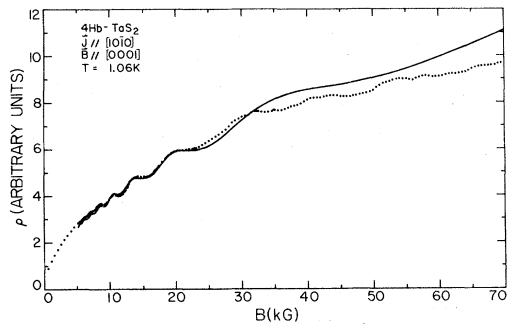

FIG. 15. Solid line represents calculated magnetresistance expected for the 0.044-MG frequency in the field range 0–70 kG. The experimental dotted curve follows the calculated curve quite well up to the approximately 30 kG and then deviates substantially at fields above 30 kG. This requires a change in the exponent for the background dc magnetoresistance. This coincides with abrupt changes in the Hall coefficient (see Fig. 7) and may indicate the onset of magnetic breakdown.

The corresponding break in the Hall-resistivity curve produces a less-negative Hall coefficient above 30 kG and at fields above 70 kG the Hall coefficient becomes positive. This can again be interpreted in terms of breakdown effects where electronlike orbits have been converted into hole-like orbits with a resulting shift in the ratio of positive and negative carriers contributing to the high-field Hall effect. If we assume the critical breakdown field to be in the range 20–30 kG and use the effective mass ratio of $\mu = 0.07$ estimated for the low frequency orbit and $E_F \sim 0.4$ eV then the corresponding energy gap is in the range 3.58×10^{-2} to 4.39×10^{-2} eV. These are only preliminary observations and more detailed analysis and model calculations will have to be carried out.

V. CONCLUSIONS

Observations of extensive quantum oscillations in the magnetoresistance and Hall effect of $4Hb$-TaS_2 and $2H$-$TaSe_2$ have been presented. Both of these layer-structure dichalcogenide materials show transitions to charge-density-wave states and at helium temperatures the evidence strongly supports the conclusion that the observed frequencies are associated with Fermi-surface sections resulting from the gapping due to the CDW formation. In $2H$-$TaSe_2$ a triple charge-density wave forms with a superlattice of $3a_0\times3a_0\times c_0$. The same superlattice should form in the trigonal prismatic layers of $4Hb$-TaS_2 and these are assumed to dominate the conductivity parallel to the layers. Fifteen frequencies in the range 0.04–8 MG has been observed in $4Hb$-TaS_2 and 11 frequencies in the range 0.8–44.6 MG have been observed in $2H$-$TaSe_2$. These correspond to cross sections of Fermi surface representing from 10^{-5} to 10^{-1} of the cross section of the original non-CDW Brillouin zone. The reduced zone of the superlattice would have an area equal to $\frac{1}{9}$ of the original zone and the required band folding would be expected to produce many small cross sections as observed in the present experiment. An initial model of the band folding by Scott and Rice[17] gives sections which are in approximate agreement with the cross sections corresponding to the observed frequencies.

The angular dependence for the majority of the frequencies as measured from the basal plane to the field direction shows a dependence of the form $\omega_\perp/\sin\theta$ which is consistent with cylindrical Fermi-surface sections exhibiting a two dimensional

character with very little k_z dependence of the energy. Magnetoresistance measurements for current along the c axis show sharp peaks when the magnetic field is in the basal plane and the relation $\Delta\rho/\rho \sim B^n$ shows exponents $n \sim 1$ while adjacent field directions show a trend toward saturation. These results are consistent with open orbits along the c axis in uncompensated metals and would be the expected behavior for the two-dimensional cylindrical Fermi surfaces proposed here.

In $4Hb$-TaS_2 the field dependence of the magnetoresistance and the abrupt changes observed in the Hall coefficient as a function of field suggest the onset of magnetic breakdown in the range 20–30 kG corresponding to an energy gap in the range $\Delta = 0.035$–0.044 eV. In contrast the magnetoresistance, Hall effect, and quantum oscillatory amplitudes in $2H$-$TaSe_2$ are well behaved up to 230 kG with no evidence of magnetic breakdown. This would be consistent with large CDW gaps as proposed by McMillan[20] for $2H$-$TaSe_2$ and also suggested by the infrared measurements of Barker *et al.*[21] which indicate a $\Delta = 0.25$ eV corresponding to a breakdown field above 200 kG even for light masses.

In the case of $4Hb$-TaS_2 unusual phase shifts in the oscillatory components are observed upon reversal of the magnetic field or current direction. These have been studied as a function of lead configuration and sample geometry and are definitely connected with the extreme conductivity anisotropy existing in the $4Hb$ phase. The existence of alternate octahedrally coordinated layers introduces tunneling conductivity along the c axis and in cases where the current flow is isolated from the potential contacts by the $1T$ layers the potential difference measured may be controlled by the tunneling path. Reversal of the magnetic field or current can introduce asymmetries in the tunneling geometry and hence phase shifts in the field-dependent potential which are different from 0 or π. A detailed model has not yet been worked out, but the effects have been well characterized and further analysis and experiment are merited.

The magnetotransport experiments reported here have clearly given direct evidence on the Fermi-surface topology connected with the charge-density-wave state of two-layer-structure materials. The key to these experiments has been the growth of more perfect crystals of the two phases used in these experiments and has demonstrated that sufficiently perfect crystals of these compounds can be produced. Further improvements of the growth technique and extension to other layer compounds and phases would certainly be in order. The band folding and resulting Fermi surfaces are so complex that direct experimental results will be required in order to allow the development of satisfactory theoretical models of the electronic structure in these materials.

ACKNOWLEDGMENTS

The authors have had useful and important discussions with Dr. T. M. Rice, Dr. F. J. DiSalvo, Dr. J. A. Wilson, Professor L. M. Falicov, Professor V. Celli, Professor C. B. Friedberg, and Professor A. W. Overhauser. The authors would like to thank Dr. F. J. DiSalvo for providing two of the $2H$-$TaSe_2$ crystals. Estelle Phillips has provided important help in the crystal-growth and measurement programs.

---

†Work supported by the U. S. ERDA Contract No. AT-(40-1)-3105.

*Work above 80 kOe was performed while the authors were Guest Scientists at the Francis Bitter National Magnet Laboratory, which is supported at MIT by the NSF.

[1]J. A. Wilson, F. J. DiSalvo, and S. Mahajan, Adv. Phys. 24, 117 (1975).

[2]A. W. Overhauser, Phys. Rev. 167, 691 (1968).

[3]D. A. Whitney, R. M. Fleming, and R. V. Coleman, Phys. Rev. B 15, 3405 (1977); R. C. Morris and R. V. Coleman, *ibid.* 7, 991 (1973); R. C. Morris, R. V. Coleman, and Rajendra Bhandari, *ibid.* 5, 895 (1972).

[4]R. M. Fleming and R. V. Coleman, Phys. Rev. Lett. 36, 1555 (1976).

[5]J. A. Wilson and A. D. Yoffe, Adv. Phys. 18, 193 (1969).

[6]H. N. S. Lee, M. Garcia, H. McKinzie, and A. Wold, J. Solid State Chem. 1, 190 (1970).

[7]John E. Graebner, Solid State Commun. (to be published).

[8]P. D. Hambourger, Phys. Rev. B 15, 1640 (1977).

[9]W. J. Wattamaniuk, J. P. Tidman, and R. F. Frindt, Phys. Rev. Lett. 35, 62 (1975).

[10]Laura M. Roth and Petros N. Argyres, in *Semiconductors and Semimetals*, edited by R. K. Willardson and Albert C. Beer (Academic, New York, 1966), p. 159.

[11]A. M. Woolley and G. Wexler (unpublished).

[12]L. F. Mattheiss, Phys. Rev. B 8, 3719 (1973).

[13]G. Wexler and A. M. Woolley, J. Phys. C 9, 1185 (1976).

[14]F. J. DiSalvo, B. G. Bagleu, J. M. Voorhoeve, and J. V. Waszcak, J. Phys. Chem. Solids 34, 1357 (1973).

[15]D. E. Moncton, J. D. Axe, and F. J. DiSalvo, Phys. Rev. Lett. 34, 734 (1975).

[16]John A. Holy, Miles V. Klein, W. L. McMillan, and S. F. Meyer, Phys. Rev. Lett. 37, 1145 (1976).

[17]G. K. Scott and T. M. Rice (unpublished).

[18]T. M. Rice and G. K. Scott, Phys. Rev. Lett. 35, 120 (1975).

[19]P. Schlottmann and L. M. Falicov, Phys. Rev. Lett. 38, 855 (1977).
[20]W. L. McMillan, Phys. Rev. B (to be published).
[21]A. S. Barker, Jr., J. A. Ditzenberger, and F. J. DiSalvo (unpublished).
[22]J. R. Anderson and D. R. Stone, in *Methods of Experimental Physics*, Vol. 11, edited by R. V. Coleman (Academic, New York, 1974), p. 33.
[23]Morrel H. Cohen and L. M. Falicov, Phys. Rev. Lett. 7, 231 (1961); and E. I. Blount, Phys. Rev. 126, 1636 (1962).
[24]L. M. Falicov and Paul R. Sievert, Phys. Rev. 138, A88 (1965).
[25]L. M. Falicov, A. B. Pippard, and Paul R. Sievert, Phys. Rev. 151, 498 (1966).